Proceedings of the EuroGNC 2013, 2nd CEAS Specialist Conference
on Guidance, Navigation & Control, Delft University of Technology,
Delft, The Netherlands, April 10-12, 2013

Design and flight testing of nonlinear autoflight control laws incorporating direct lift control

Thomas Lombaerts and Gertjan Looye

Abstract This publication describes how direct lift control has been incorporated in a nonlinear autoflight control algorithm. Direct lift control demonstrated its use in earlier aircraft designs. In two recent internal DLR projects, accurate flight path tracking in atmospheric disturbances was an important research goal, where direct lift control could potentially provide an important contribution. In these projects, use has been made of nonlinear control techniques. Objective of this research publication is to incorporate direct lift control in these nonlinear control laws. Simulations as well as flight tests have shown that more accurate flight path changes are achieved by this addition. Direct lift control can be particularly useful for path tracking as well as in turbulent air, since it facilitates lift changes without pitching. More precisely, the non-minimum phase behaviour of the aircraft caused by the elevators is eliminated in this way.

1 Introduction

Besides the regular control surfaces which can be found on a conventional aircraft wing, such as (high and low speed) ailerons, flaps, slats and speedbrakes or spoilers, some specific aircraft types have an additional control capability at the trailing edge of the wing to influence lift directly, this is called direct lift control (DLC). For most of the latter aircraft, DLC is provided by means of the spoilers in the lower deflection ranges, such as is the case for the Lockheed L-1011 Tristar civil airliner [14], the Boeing C-17 Globemaster III military airlifter, and the aircraft-carrier based jets the Grumman F-14 Tomcat and the Lockheed S-3 Viking. Their use is to manage sink rate finely so that a more accurate and smoother glideslope can be flown. This is done through the lift force directly instead of indirectly through the angle of attack

Thomas Lombaerts · Gertjan Looye
German Aerospace Center DLR, Institute of System Dynamics and Control, Münchner Straße 20, 82234 Weßling, Germany, e-mail: thomas.lombaerts@dlr.de e-mail: gertjan.looye@dlr.de

α and subsequently the pitch rate q, which takes more time. As a result, direct lift control facilitates lift changes without pitching. More precisely, the non-minimum phase behaviour of the aircraft caused by the elevators is eliminated in this way. This is especially useful during the approach. In the literature, many possible purposes have been mentioned for direct lift control, namely flight path tracking[6], station keeping for in flight refueling[15] and increasing passenger comfort during turbulence[5]. Ref. [7] makes a comparative analysis of different control strategies for the use of continuously variable trailing edge control surfaces during landing. This history confirms the efficiency of direct lift control for flight guidance.

Two recent internal DLR projects focus on flight guidance, namely "Wetter-und-Fliegen" and "TOPGAL". "Wetter-und-Fliegen" (completed in 2011) aimed at augmenting safety and efficiency of air transport. This high-level goal has been achieved by building systems for automatic control to increase the performance of the aircraft when confronted with wind gusts, wake vortices and thunderstorms. TOPGAL (Total Performance System for GBAS (Ground Based Augmentation System) based Automatic Landings, completed in 2012) investigates GBAS based navigation in conjunction with flight management and autopilot systems. A so-called Ground Based Augmentation System enables aircraft to use satellite navigation for guidance on a precision approach. In both projects, accurate path tracking and atmospheric disturbance rejection are important research aspects. It is especially in this context that direct lift control can provide an important contribution, as the aforementioned history has shown.

In the VFW-614 based ATTAS laboratory aircraft (Advanced Technologies Testing Aircraft System) of DLR, a direct lift control capability has been included primarily for the purpose of in-flight simulation, however they can also be used for autoflight guidance. ATTAS has DLC flaps as part of the landing flaps, which makes them only usable at flap settings 1, 5 and 14. ATTAS's direct lift control capability provides an opportunity for the flight guidance research in the internal DLR projects "Wetter-und-fliegen" and "TOPGAL". In this context, a set of nonlinear autoflight control laws incorporating direct lift control has been designed and flight tested on ATTAS. This is an extension of a previously developed set of nonlinear flight control laws, which has been presented in Ref. [11]. This latter autoflight control algorithm is based on three consecutive dynamic inversion loops, which have been separated by means of the principle of time scale separation. This control setup can be augmented for flight path control by making use of the direct lift control flaps. This augmentation serves a double purpose. First, aircraft responses to flight path angle commands are made faster and more accurate. Secondly, turbulence induced disturbances are rejected to improve passenger comfort, as will be shown in the results. The purpose of the paper is to show the integration of the concept of direct lift control in nonlinear autoflight control laws.

Section 2 provides a description of the simulation model of the ATTAS laboratory aircraft. A summary of the benchmark nonlinear autoflight controller structure is given in section 3, while the improvement of direct lift control is elaborated in section 4. Simulation results and flight test results are given in sections 5 and 6. Finally, section 7 provides some conclusions and recommendations.

2 Description ATTAS model

This section describes the high fidelity aircraft simulation model which has been constructed using the Modelica Flight Dynamics Library [13]. The aircraft is the flying test-bed ATTAS (Advanced Technologies Testing Aircraft System) [3]), which is operated by the German Aerospace Center (DLR). ATTAS is based on a VFW 614, a small 44-passenger civil transport aircraft with two Rolls-Royce turbofan engines mounted on top of the wings, a wing span of 21.5 m and a length of 25 m, as shown in Fig. 1. This simulation model was originally developed in the frame of the EU project REAL [18] for automatic landing control laws design and is the basis for the flight control law design described in this paper.

Fig. 1 DLR VFW-614 ATTAS in flight; source: DLR

The ATTAS model has been implemented using the object-oriented modeling language Modelica and the Flight Dynamics Library, developed at the department of Robotics and Mechatronics. An object diagram showing the most important components is depicted in Fig. 2. From this model, simulation and design analysis models are automatically generated, as well as the inner core of the Nonlinear Dynamic Inversion-based flight control laws [13].

The ATTAS simulation model includes flight dynamics, systems and environment models. The most important components are briefly described below. These descriptions focus on aspects relevant for the purpose of control design.

Aerodynamics

Aerodynamic model equations have been defined for typical aerodynamic variables like angle of attack α, angle of side slip β, true airspeed V_{TAS}, Mach number M, etc. For this, ATTAS-specific aerodynamic coefficient data have been implemented[1, 4]. In addition, multiplicative uncertainty has been added to the aerodynamic model coefficients in order to cover potential differences with the actual aerodynamics.

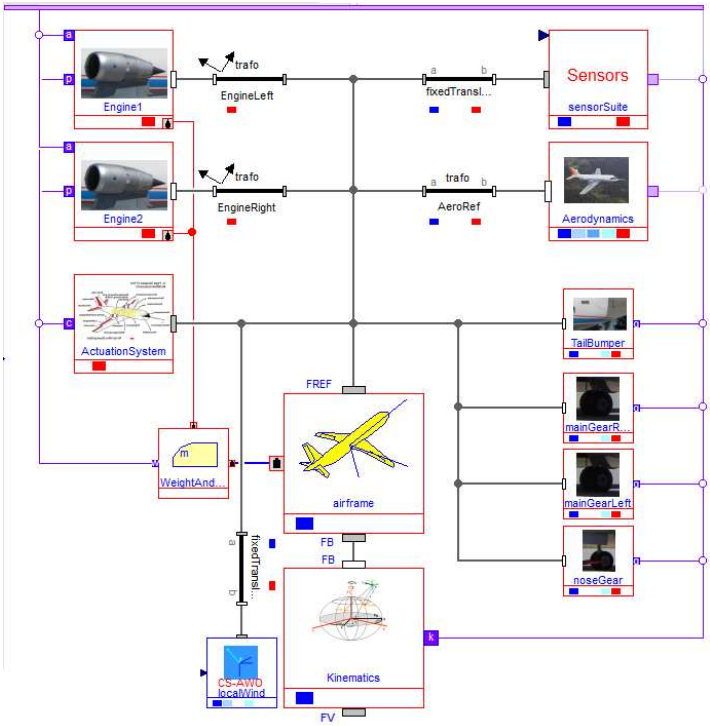

Fig. 2 Modelica object diagram with the most important ATTAS components

Propulsion

The ATTAS is equipped with Rolls-Royce turbofan engines. In this component, the thrust is computed and equations of motion for engine shaft dynamics are taken into account, including effects such as hysteresis in the fuel control unit.

Actuator dynamics

The ATTAS is amongst others equipped with ailerons, rudder, elevators and a trimmable horizontal stabiliser. These surfaces are driven by hydraulic actuators, which have been modelled as first order transfer functions with rate and position limits. Speed dependent deflection command limiting has been incorporated as well. Moreover, a flight control system signal transport delay of 150*ms* (including multiplicative uncertainty) has been added in the aileron, elevator and rudder channels.

Sensor dynamics

The ATTAS is equipped with a range of sensors for air data, inertial measurements (accelerometers, etc.), guidance (ILS, Radio altitude), etc. These sensors are com-

bined into a sensor system model. As far as the air data sensors are concerned, there are two alternatives to measure the angle of attack α. This will be elaborated further. The sensor dynamics are modelled by first order transfer functions representing the sensor lag. When the conventional vanes are used to measure the angle of attack α, an additional transport delay of 300ms has to be incorporated as well. For some measurement data, quantizer effects or noise is added. For example, when the angle of attack sensor of ATTAS is on a long nose boom, its flexibility adds a 6 Hz disturbance to the signal. For this reason, the signal has to be combined with inertial measurements using complementary filtering techniques as explained by Looye[13]. The relevance of these dynamics and disturbances for specific measurements is shown in table 1.

sensed quantity	variables	sensor lag	delay	quantizer effect	noise type
speed (various)	V	✓		✓	
body angular rates	p, q, r	✓			
load factors	n_x, n_y, n_z	✓			
Euler angles and course	ϕ, θ, ψ, χ	✓		✓	
aerodynamic angle (nose boom)	α	✓			sine form
aerodynamic angle (vanes)	α	✓	✓		
flight path angle	γ	✓		✓	
fan speed	$N1$				white noise

Table 1 Instrumentation error information for measuring equipment

Mind that raw measurement data contain much more disturbance effects, e.g. raw inertial measurements from gyros and accelerometers are always perturbed by a bias and noise. However, the research presented in this paper considers a loosely coupled flight instrumentation system, using processed observations as opposed to the tightly coupled counterpart with raw measurement data.

Wind and turbulence

Wind as well as turbulence have been incorporated in the simulation model. Wind is treated here as a stationary phenomenon. Turbulence is a stochastic process that can partially be defined by power spectra of the velocity components. Turbulence is modeled by the commonly used Dryden spectra[16].

3 Autoflight controller structure

The autoflight controller consists of three consecutive dynamic inversion loops, based on the concept of time scale separation, as illustrated in Fig. 3. The inner dynamic inversion loop is in common with the manual control law. The middle and outer control loops are autoflight specific. The inner loop is based on the aircraft dy-

namics, and is therefore aircraft specific. The second loop is based on the kinematics and thus independent of aircraft type. Finally, the third loop consists of a kinematic (from navigation quantities towards bank angle and symmetric aerodynamic forces) as well as a dynamic part (from symmetric aerodynamic forces towards aerodynamic angles). The commanded sideslip angle in the second loop is typically zero, and does not appear therefore in the outer loop[1]. The commanded quantities in the outer loop: course angle χ, flight path angle γ and speed ΔV are typical navigation quantities for waypoint guidance. Mind that the dynamic part of the control setup complies with the principle of time scale separation, since the aerodynamic moments have typically a higher bandwidth than the aerodynamic forces.

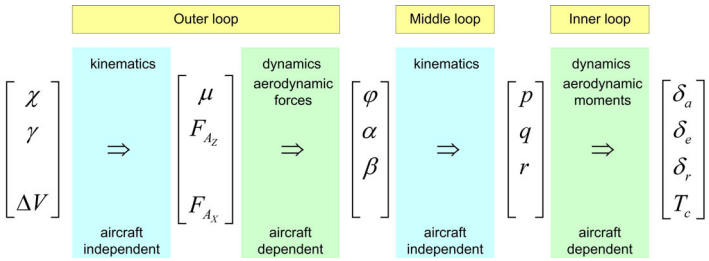

Fig. 3 Global overview of the time scale separation based control setup

In the next sections, the control laws in the inner, middle and outer control loop are given. Each loop consists of a dynamic inversion control, a first or second order linear controller and a first order reference model. More detailed explanations about the concept of nonlinear dynamic inversion and the control loops as they have been implemented here, and how they were derived, can be found in Ref. [8, 11].

Inner control loop

The inner control loop for angular rate control is defined as follows [9]:

$$\begin{bmatrix} \delta_a \\ \delta_e \\ \delta_r \end{bmatrix} = \begin{bmatrix} b\tilde{C}_{l_{\delta_a}} & 0 & b\tilde{C}_{l_{\delta_r}} \\ 0 & \overline{c}\tilde{C}_{m_{\delta_e}} & 0 \\ b\tilde{C}_{n_{\delta_a}} & 0 & b\tilde{C}_{n_{\delta_r}} \end{bmatrix}^{-1} \cdot \left\{ \frac{\mathbf{I}}{\frac{1}{2}\rho V^2 S} \left(\begin{bmatrix} \nu_p \\ \nu_q \\ \nu_r \end{bmatrix} + \mathbf{I}^{-1} \begin{bmatrix} p \\ q \\ r \end{bmatrix} \times \left(\mathbf{I} \begin{bmatrix} p \\ q \\ r \end{bmatrix} \right) \right) - \begin{bmatrix} bC_{l_{\text{states}}} \\ \overline{c}C_{m_{\text{states}}} \\ bC_{n_{\text{states}}} \end{bmatrix} \right\} \quad (1)$$

[1] Note that, due to the setup of the control laws and the nature of dynamic inversion, this can still lead to non-zero steady state values of β, as long as they are in balance with steady state roll angle ϕ and lateral specific force A_y, such that the first order time derivative of the sideslip angle $\dot{\beta} = 0$, see also Ref. [8].

where the virtual inputs $\begin{bmatrix} \nu_p & \nu_q & \nu_r \end{bmatrix}^T$ are the time derivatives of the rotational rates of the aircraft, which are selected to be the control variables in order to obtain rate control. They are provided by the first order linear controllers as shown in eq. (2) – (4). The first part of eq. (1) performs the control inversion, while the second part contains the state inversion.

It should be noted that this dynamic inversion is not perfect due to the presence of the multiplicative uncertainties in the aerodynamic model as already explained in section 2. However, the linear controller has shown to be capable to deal with these modeling errors, as can be seen in sections 5 and 6.

The first order linear controllers have the following control laws:

$$\nu_p = K_p \left(p_{\text{ref}} - p_m \right) + \dot{p}_{\text{ref}} \tag{2}$$

$$\nu_q = K_q \left(q_{\text{ref}} - q_m \right) + \dot{q}_{\text{ref}} \tag{3}$$

$$\nu_r = K_r \left(r_{\text{ref}} - r_m \right) + \dot{r}_{\text{ref}} \tag{4}$$

The first order reference models are defined as follows:

$$p_{\text{ref}} = \frac{1}{T_p s + 1} p_{\text{comm}}, \quad q_{\text{ref}} = \frac{1}{T_q s + 1} q_{\text{comm}}, \quad r_{\text{ref}} = \frac{1}{T_r s + 1} r_{\text{comm}} \tag{5}$$

The interconnection of aircraft model, dynamic inversion control laws, first order linear controllers and first order reference models is shown in Fig. 4. The feedforward channel of the first order time derivative from reference model to the linear controller is visible here and eliminates a time delay which would otherwise be present in the tracking of the reference signal.

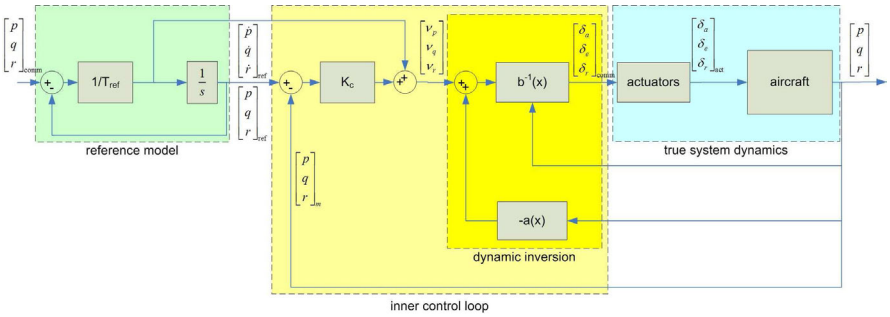

Fig. 4 Interconnection of aircraft model, dynamic inversion control laws, controllers and reference models

The parameter values, for time constants as well as control gains, are enumerated in Tab. 2. In the next sections, the control laws in the middle and outer control loop will be given.

Middle control loop

From the theory of flight dynamics, see ref. [17], the overall second level NDI control law is:

$$\begin{bmatrix} p_{\text{comm}} \\ q_{\text{comm}} \\ r_{\text{comm}} \end{bmatrix} = \begin{bmatrix} 1 & \sin\phi\tan\theta & \cos\phi\tan\theta \\ -\frac{v_b}{\sqrt{V^2-w_b^2}} & \frac{u_b}{\sqrt{V^2-w_b^2}} & 0 \\ \frac{w_b}{\sqrt{V^2-v_b^2}} & 0 & \frac{-u_b}{\sqrt{V^2-v_b^2}} \end{bmatrix}^{-1} \cdot \left\{ \begin{bmatrix} \nu_{\dot{\phi}} \\ \nu_{\dot{\alpha}} \\ \nu_{\dot{\beta}} \end{bmatrix} - \begin{bmatrix} 0 \\ -\frac{1}{\sqrt{V^2-w_b^2}}\left(A_z + g\cos\theta\cos\phi\right) \\ \frac{1}{\sqrt{V^2-v_b^2}}\left(A_y + g\cos\theta\sin\phi\right) \end{bmatrix} \right\} \tag{6}$$

where the virtual inputs $\begin{bmatrix} \nu_{\dot{\phi}} & \nu_{\dot{\alpha}} & \nu_{\dot{\beta}} \end{bmatrix}^T$ are the time derivatives of the roll angle and aerodynamic angles of the aircraft, which are selected to be the control variables in order to obtain angle control. They are provided by the first order linear controllers as shown in eq. (7) – (9).

The linear controllers have the following control laws:

$$\nu_{\dot{\phi}} = K_\phi\left(\phi_{\text{ref}} - \phi_m\right) + \dot{\phi}_{\text{ref}} \tag{7}$$

$$\nu_{\dot{\alpha}} = K_\alpha\left(\alpha_{\text{ref}} - \alpha_m\right) + \dot{\alpha}_{\text{ref}} \tag{8}$$

$$\nu_{\dot{\beta}} = \left(K_\beta + \frac{K_{\beta_I}}{s}\right)\left(\beta_{\text{ref}} - \beta_m\right) \tag{9}$$

The first order reference models are defined as follows:

$$\phi_{\text{ref}} = \frac{1}{T_\phi s + 1}\phi_{\text{comm}}, \quad \alpha_{\text{ref}} = \frac{1}{T_\alpha s + 1}\alpha_{\text{comm}}, \quad \beta_{\text{ref}} = 0 \tag{10}$$

The parameter values, for time constants as well as control gains, are enumerated in Tab. 2.

Outer control loop

The command laws in the outer loop for the symmetric forces in the aerodynamic frame of reference $F_{A_{X_{\text{comm}}}}, F_{A_{Z_{\text{comm}}}}$ and the roll angle μ are [8, 11]:

$$\mu_{\text{comm}} = \arctan\left(\frac{\dot{\chi}_{\text{comm}}\cos\gamma}{\dot{\gamma}_{\text{comm}} + g\frac{\cos\gamma}{V}}\right) \tag{11}$$

$$F_{A_{X_{\text{comm}}}} = m\left(\dot{V}_{\text{comm}} + g\sin\gamma\right) \tag{12}$$

$$F_{A_{Z_{\text{comm}}}} = \sqrt{F_{\text{required}}^2 - F_{A_Y}^2}$$
$$= -\cos\gamma \sqrt{m^2 \left[\left(g + \frac{V\dot{\gamma}_{\text{comm}}}{\cos\gamma} \right)^2 + (V\dot{\chi}_{\text{comm}})^2 \right] - \left(\frac{F_{A_Y}}{\cos\gamma} \right)^2} \quad (13)$$

where $\mu_{\text{comm}} \approx \phi_{\text{comm}}$ and $F_{A_{X_{\text{comm}}}}, F_{A_{Y_{\text{comm}}}}, F_{A_{Z_{\text{comm}}}}$ are the combined aerodynamic and thrust force components in the aerodynamic frame of reference. The quantities $\left[\dot{V}_{\text{comm}}\ \dot{\gamma}_{\text{comm}}\ \dot{\chi}_{\text{comm}}\right]^T$ are the time derivatives of the navigation quantities of the aircraft, which are selected to be the control variables in order to obtain navigation control. They are provided by the second order linear controllers as shown in eq. (17) – (19).

The command laws for angle of attack and thrust coefficient are as follows:

$$\alpha_{\text{comm}} = \frac{-\frac{F_{A_{Z_{\text{comm}}}}}{0.5\rho V^2 S} - C_{L_0} - C_{L_{LG}} LG}{\left(C_{L_{\alpha,WF}} + C_{L_{\alpha,M,WF}} M\right) Y + \frac{S_h}{S_w}\left(C_{L_{\alpha_h}} + C_{L_{\alpha_{Mh}}}(M-0.3)\right)\left(1 - \frac{\partial \varepsilon_h}{\partial \alpha}\right)} \quad (14)$$

$$\text{where:} \quad Y = \left(\frac{1}{4}\left(1 + \sqrt{X}\right)^2\right), \ X = \frac{1}{2}\left(1 - \tanh\left(C_1\left(\alpha_m - \tau_2\dot{\alpha}_m - \alpha^*\right)\right)\right) \quad (15)$$

$$T_{C_{\text{comm}}} = \frac{F_{A_{X_{\text{comm}}}} + C_D 0.5\rho V^2 S}{\cos(\alpha - 3^\circ)} \quad (16)$$

with $C_{L_\bullet}$ the aerodynamic derivatives for the lift force, 'LG' stands for 'landing gear', 'WF' depicts 'wing-fuselage combination', S_h and S_w are the surface areas of horizontal stabilizer and wing respectively. ε_h is the downwash at the horizontal stabilizer. α_m is the measured angle of attack and α^* is the angle of attack at $X = 0.5$. X is the location on the wing where the airflow separates. The first and second order linear controllers have the following control laws:

$$\dot{V}_{\text{comm}} = \left(K_V + \frac{K_{V_I}}{s}\right)(V_{\text{ref}} - V_m) \quad (17)$$

$$\dot{\gamma}_{\text{comm}} = \left(K_\gamma + \frac{K_{\gamma_I}}{s}\right)(\gamma_{\text{ref}} - \gamma_m) + \dot{\gamma}_{\text{ref}} \quad (18)$$

$$\dot{\chi}_{\text{comm}} = K_\chi(\chi_{\text{ref}} - \chi_m) + \dot{\chi}_{\text{ref}} \quad (19)$$

where a limited integrator has been used in the speed controller in order to prevent windup effects.

The first order reference models are defined as follows:

$$V_{\text{ref}} = \frac{1}{T_V s + 1} V_{\text{comm}}, \quad \gamma_{\text{ref}} = \frac{1}{T_\gamma s + 1}\gamma_{\text{comm}}, \quad \chi_{\text{ref}} = \frac{1}{T_\chi s + 1}\chi_{\text{comm}} \quad (20)$$

The commanded values for speed, flight path angle and course are provided by the pilot through the mode control panel. The parameter values, for time constants as well as control gains, are enumerated in Tab. 2.

Control gains

The parameter values for the three control loops are given in Tab. 2. The principle of time scale separation can be observed in this table.

Navigation loop		Aerodynamic loop		Rate loop	
Time constants	Control gains	Time constants	Control gains	Time constants	Control gains
$T_\chi = 0.2$	$K_\chi = 0.4$	$T_\phi = 1.8$	$K_\phi = 0.4653$	$T_p = 2.8$	$K_p = 3.4$
$T_\gamma = 0.4$	$K_{\gamma_P} = 0.9$	$T_\alpha = 1.8$	$K_\alpha = 2.3025$	$T_q = 2.8$	$K_q = 1.1735$
	$K_{\gamma_I} = 0.1$				
			$K_{\beta_P} = 0.9163$	$T_r = 2.8$	$K_r = 2.3$
			$K_{\beta_I} = 0.8167$		
$T_V = 0,1$	$K_{V_P} = 0.35$				
	$K_{V_I} = 0.05$				

Table 2 Parameter values for time constants and control gains

4 Direct Lift Control flaps

The autoflight controller as discussed in section 3 can be extended by means of the direct lift control flaps. Since they have a direct influence on the lift force, without non-mimum phase transient as is the case with the elevator, they can improve the agility of the aircraft. As a consequence, the slightly modified global overview is illustrated in Fig. 5.

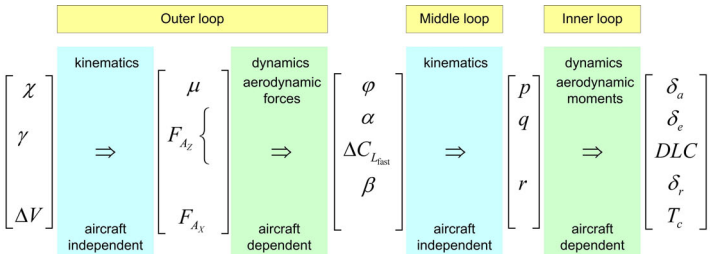

Fig. 5 Global overview of the control setup including direct lift control

Influence of DLC on lift force

The direct lift control flaps (DLC) have a third order influence on the lift force C_L. From ref. [4], this influence can be represented by the following relationship:

$$\Delta C_{L_{DLC}} = 2\left(L_1\delta_{DLC} + L_2\delta_{DLC}^2 + L_3\delta_{DLC}^3\right)$$

The DLC's are operational in flight conditions with flaps 1, 5, and 14. Their nonlinear influence on the lift is illustrated in Fig. 6. This has been implemented in a look up table for DLC deflection ranges between -30° and $+20^\circ$. Inverse table lookup is allowed to extrapolate. The computed control deflections are then allowed up to the aforementioned saturation limits.

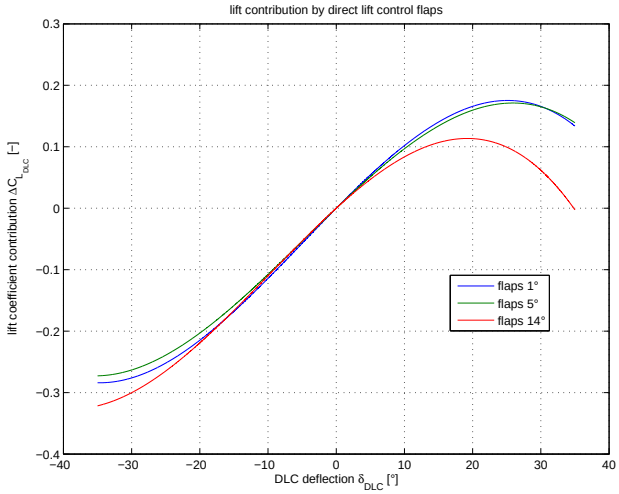

Fig. 6 Lift contribution by direct lift control flaps

DLC control law

The third order relationship above can be used as a nonlinear mapping from DLC flap deflection towards lift force contribution. Inverse implementation in the flight control law can be achieved by a lookup table. Since the reference model for the angle of attack α is in fact a first order filter, the autoflight commanded angle of attack is actually low-pass filtered while processed through the α reference model. Simultaneously, the remaining lift force component to be provided by the DLC's is defined as:

$$\Delta C_{L_{DLC_{\text{comm}}}} = C_{L_\alpha}(\alpha_{\text{comm}} - \alpha_m) \tag{21}$$

where α_{comm} is unfiltered. Based upon this lift component contribution, the required DLC deflection is calculated by means of the earlier mentioned lookup table. An

overview of this direct lift control setup is given in Fig. 7. Since direct lift control acts complementary to the slower angle of attack α (because of the low pass filtering in the reference model), its behaviour has in fact washout characteristics. Adding DLC increases significantly the γ channel bandwidth. Experiment results shown in sections 5 and 6 will illustrate the beneficial influence of these DLC flaps.

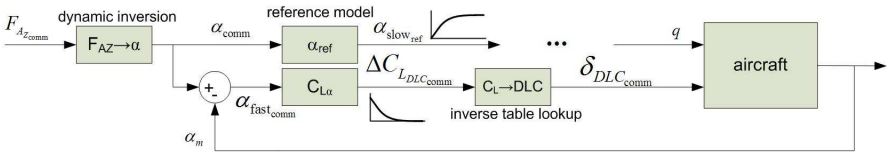

Fig. 7 Frequency based distribution of commanded vertical aerodynamic force $F_{A_{Z_{comm}}}$ over slower reference angle of attack $\alpha_{slow_{ref}}$ and faster direct lift control flap deflection δ_{DLC}

5 Simulation results

Simulations have been included to demonstrate the beneficial influence of direct lift control on tracking performance as well as atmospheric disturbance rejection.

5.1 Tracking performance of direct lift control

A change in flight path angle $\Delta\gamma = 3^\circ$ has been commanded in the simulations, with and without direct lift control. The simulations can be found in Fig. 8. Figure 8(a) shows the situation without direct lift control contribution. The flight path angle change is achieved by the elevator only. A time delay in and minimal initial opposite response (so-called non minimum phase behaviour) of the flight path angle γ can be seen. The reason for this is explained in Fig. 9(a). The elevator deflects upward ($\delta_e < 0$ in Fig. 8(a)), which causes an instant and brief decrease in total lift on the aircraft ($\Delta L_{\text{tail}} < 0$ in Fig. 9(a)). Simultaneously, a pitch up moment $M > 0$ is generated, which sets off a sequence of positive pitch rate $q > 0$, positive change in angle of attack ($\Delta\alpha > 0$), positive lift change $\Delta L > 0$ and thus a climbing flight path angle $\gamma > 0$. Due to the principle of time scale separation, as illustrated in Fig. 3, this sequence causes a time delay.

Figure 8(b) illustrates the aircraft response with direct lift control. The flight path angle change is achieved by cooperating elevator and DLC flaps. The response tracks the reference signal γ_{ref} very accurately. Complementary to the elevator action, which takes some time to build up a change in flight path angle, the DLC flaps act as a washout filter. As illustrated in Fig. 9(b), the downward deflection of the DLC flaps ($\delta_{DLC} > 0$ in Fig. 8(a)) has a direct influence on the total lift of the air-

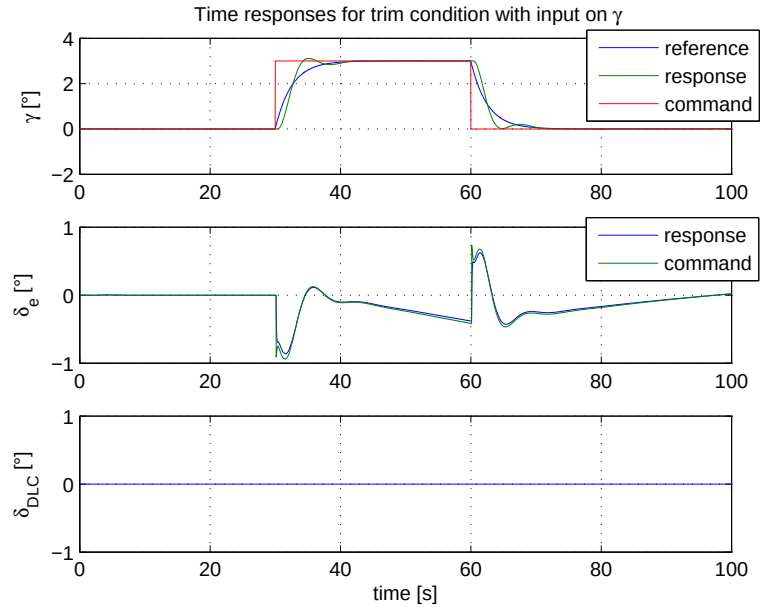

(a) γ captures without DLC

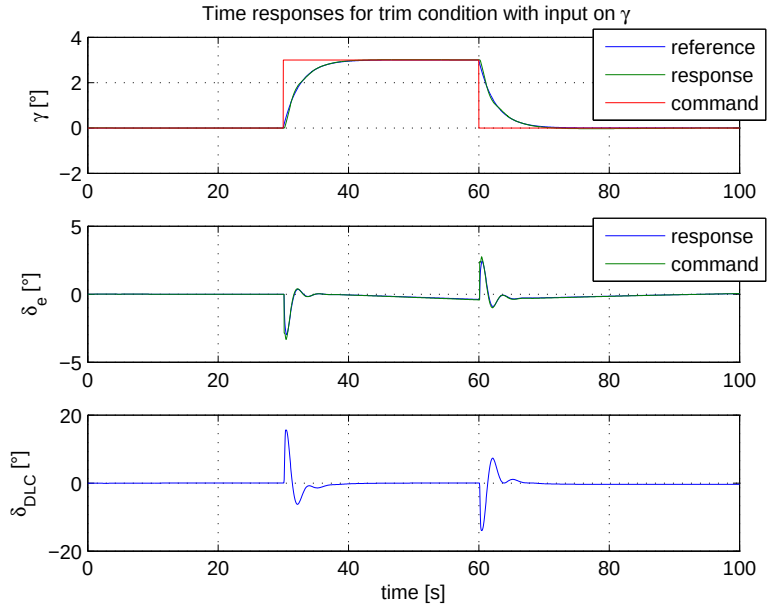

(b) γ captures with DLC

Fig. 8 Comparison of time responses of flight path angle captures with and without direct lift control

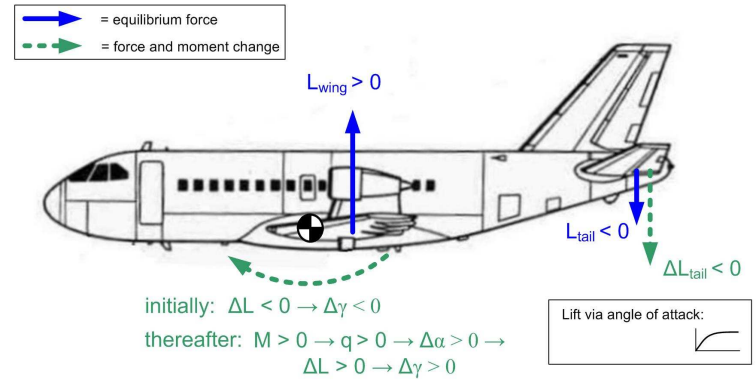

(a) elevator induced climb

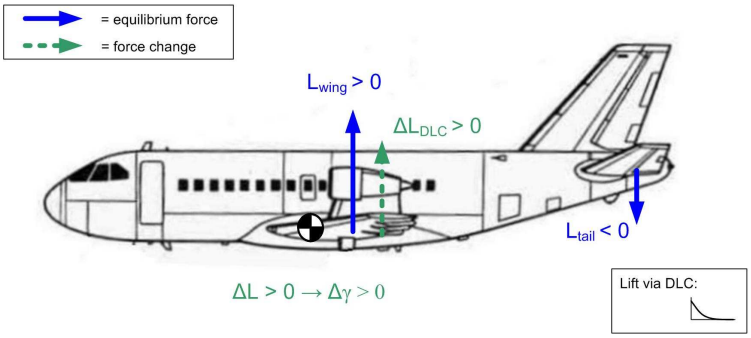

(b) DLC flap induced climb

Fig. 9 Comparison of climb dynamics induced by elevator or DLC flaps

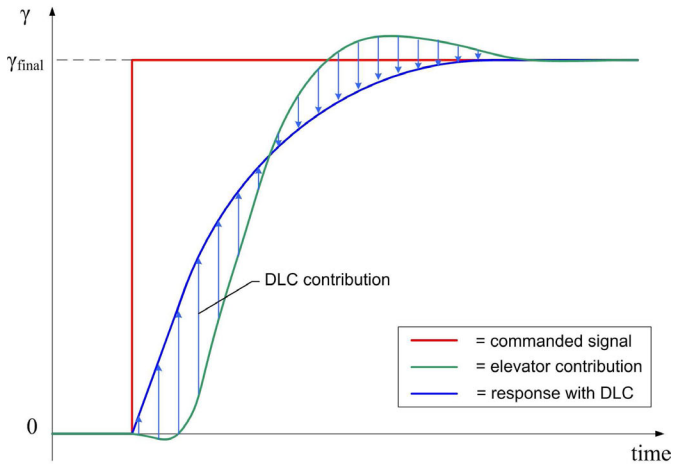

Fig. 10 Elevator and DLC contributions to flight path angle change

craft $\Delta L > 0$ and thus generates a climbing flight path angle $\gamma > 0$ without time delay and without pitching. Fig. 5 illustrates this as well in the perspective of time scale separation. As can be seen in Fig. 8(b), the DLC flaps have only an intermediate short term "washout" influence to eliminate the time delay and non-minimum phase effect of the elevators. The elevator action is still dominant in the longer term. This is also illustrated in Fig. 10.

5.2 Turbulence disturbence rejection of direct lift control

Besides improving the tracking performance, direct lift control can contribute in atmospheric disturbance rejection, since it reacts faster on tracking errors. However, this could not be verified during the test flight, since no turbulence has been encountered. Therefore, turbulence has been activated in the computer simulations. Two simulation runs have been made through the same turbulence profile, with and without direct lift control activated. During these level flight simulation runs, zero flight path angle was being tracked. Fig. 11 compares the time histories of flight path angle γ and pitch attitude angle θ during this 80s simulation runs. From the figure, it can be seen that the time responses have in general smaller turbulence induced peaks, which is caused by DLC. This confirms that direct lift control effectively reduces turbulence induced disturbances and as such increases passenger comfort.

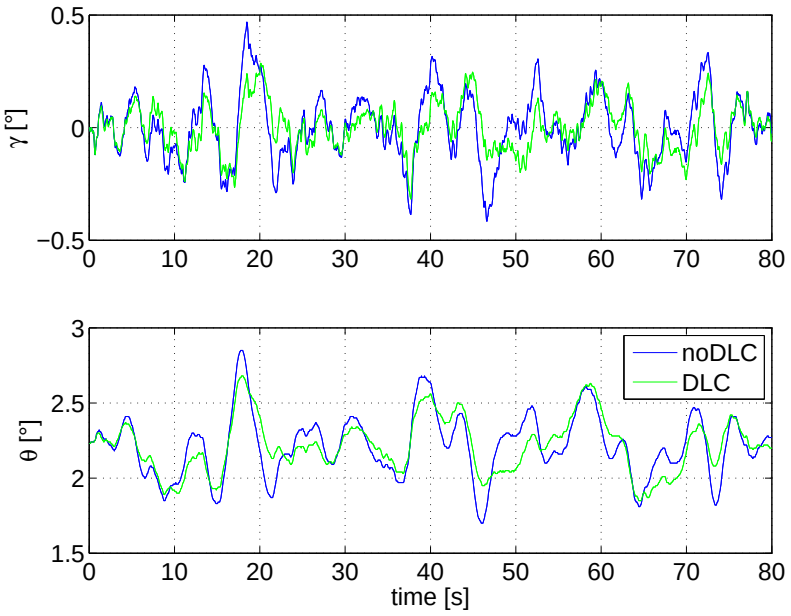

Fig. 11 Turbulence handling with and without DLC

6 Flight test results

On November 3 2011, a flight test has been performed to evaluate the performance of the nonlinear autoflight control system in a relevant environment. First the ATTAS laboratory aircraft will be introduced. Thereafter the experiment procedure is explained. Finally, the flight test results are shown.

6.1 ATTAS flying laboratory

The aforementioned flying test-bed ATTAS (Advanced Technologies Testing Aircraft System) of DLR has been used for this test flight. ATTAS is based on a VFW 614, a 44-passenger civil transport aircraft. The original conventional mechanical control system of the basic aircraft was supplemented by the German aerospace industry (MBB) and the DLR with an electrical flight control system (Fly-By-Wire). Figure 12(a) shows an overview of the aircraft and which control effectors can be steered through the fly-by-wire system. If the ATTAS electronic flight control system is used, the safety pilot can go back to the mechanical control system at any time by pressing the safety switch. In this perspective, the safety pilot is the central instance of the ATTAS safety concept. As such, the mechanical control system of the basic aircraft is the backup system of the electric flight control system.

The left hand side cockpit controls (evaluation pilot's seat) are disconnected from the right hand side mechanical basic aircraft controls of the safety pilot. The evaluation pilot has a two-axes sidestick, shown in fig. 12(b), FBW-thrust levers, a landing flap lever, and programmable electronic primary and navigational displays available. The fly-by-wire systems architecture comprises full dual redundant control systems with four computers in each of both lanes.

The fully fueled aircraft can load 3.5 tons of test equipment. Additional to the standard control surfaces ATTAS has six direct lift control (DLC) flaps at the trailing edge of the landing flaps. These flaps permit a very fast influence on the lift. ATTAS has a maximum cruising altitude which amounts to 25000 feet (7620 m) and its maximum cruising speed is 288 knots (148.2 m/s, CAS). Furthermore, ATTAS has a very low landing speed of about 100 knots (51.4 m/s). Due to its size, its relatively spacious cabin, its additional load capacity and its flight characteristics the VFW 614 is an ideal flying test-bed for various applications. Active flight control is one of the most sophisticated fields of research of ATTAS, research results have been presented in ref. [2, 12]. Recently, flight test results of nonlinear manual and autoflight control in ATTAS have been presented in [10, 11].

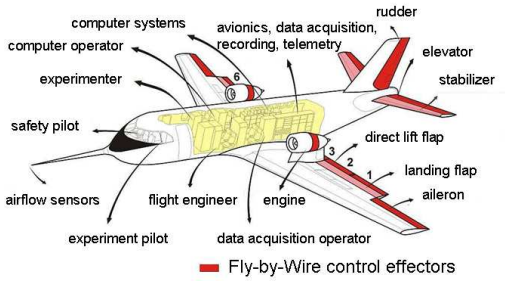

(a) An overview of the technical modifications incorporated in ATTAS. Besides the conventional elevator, rudder, and aileron control surfaces, the engines, six direct lift control flaps, landing flaps, and stabilizer are under fly-by-wire (FBW) control. Source: DLR

(b) ATTAS cockpit view, with experiment pilot seat on the left and safety pilot seat on the right; Source: DLR

Fig. 12 DLR VFW-614 ATTAS

6.2 Experiment procedure

The DLC related experiments have been performed in one flight condition. Altitude was around FL150, speed regime was 180 KIAS with flaps 1°, gear was up and spoilers in. Autotrim and autothrottle were both active during the tests. After taking off at Braunschweig Airport, ATTAS has flown north to the coastline of the Baltic Sea, and then south back to the airport, as illustrated in fig. 13. The experiments have been performed throughout the whole flight.

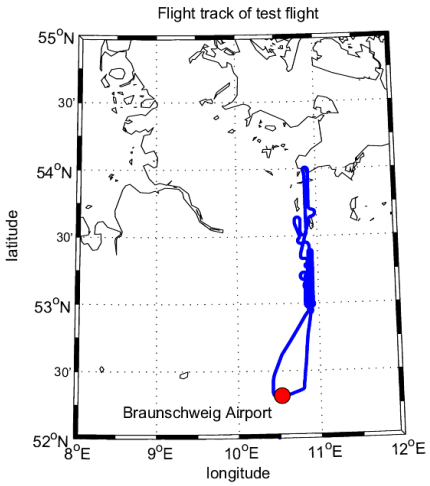

Fig. 13 Flight track of test flight, date: 3/11/2011

During the experiments, the evaluation pilot executed various flight path angle captures in order to verify the performance of the tracking mode with and without DLC. These captures are initiated by the experiment pilot through the mode control panel. In order to obtain pure step commands, an activation switch has been incorporated as well, which needs to be pressed after the requested value for the angle change has been dialed. More information about the other captures and experiments during this flight can be found in Ref. [11].

6.3 Results

The flight path angle captures are shown in Fig. 14. The oscillating behaviour of the flight path angle after angle capture is caused by the perturbing autotrim actions. The influence of the direct lift control (DLC) flaps is illustrated in Fig. 14(a). The corresponding elevator and direct lift control surface actions can be seen in Fig. 14(b). By comparing the graphs in Fig. 14, it can be seen that the DLC's assist in tracking the reference flight path angle γ_{ref} more accurately. Comparing the direct lift control surfaces with the elevator behaviour in Fig. 14(b) reveals opposite deflections. This is because the DLC's have a direct influence on the lift force, and thus on the flight path angle. This is more efficient than the elevator, which influences the lift force primarily through the angle of attack, which causes a time delay in the responses. Moreover, non minimum phase behaviour is present between elevator and lift force, which is not the case for the DLC's.

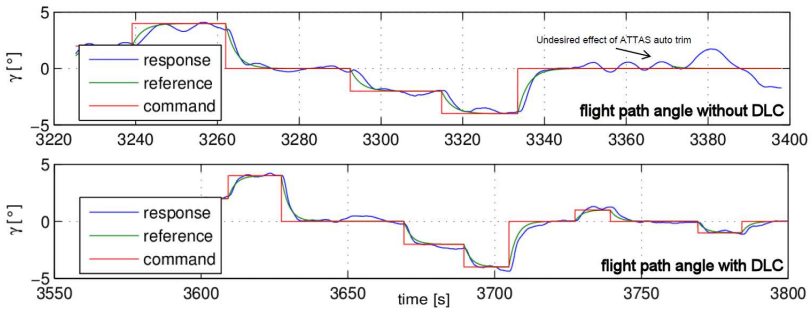

(a) captures at 180 KIAS and flaps 1, DLC off and on

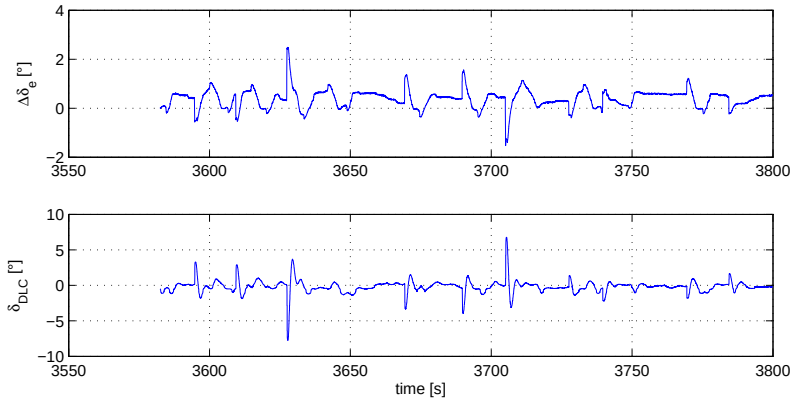

(b) corresponding elevator and DLC deflections

Fig. 14 Flight path angle captures with and without direct lift control

7 Conclusions and recommendations

An improvement to previously developed nonlinear autoflight control laws has been designed, based on direct lift control. The previously developed nonlinear dynamic inversion based control laws are built up in a modular way consisting of three layers, according to the principle of time scale separation. As such, adaptation of the controller to different aircraft types does not require major conversion work of the controller. The extension with direct lift control adds an additional control channel in this setup and preserves the modular structure. These control laws have been flight tested on the DLR ATTAS fly-by-wire testbed. Flight tests have shown that direct lift control assists in tracking the flight path angle γ more accurately, since time delays and non-minimum phase behaviour are effectively eliminated. More precisely, direct lift control assists in establishing flight path angle changes without time delay and without pitching. Moreover, the system increases flight path accuracy as well as passenger comfort during turbulence, by reducing turbulence induced perturbations of the flight path angle γ as well as of the pitch attitude angle θ.

This direct lift control strategy has been designed for and flight tested in the ATTAS fly-by-wire testbed, since this aircraft has dedicated direct lift control flaps, as explained in the introduction. Currently planned new aircraft designs have no dedicated direct lift control flaps. However, the results which have been obtained in this research warrant further investigations if the same performance could be achieved by steering the spoilers or similar appropriate control surfaces on the aircraft wing in a symmetrical manner.

8 Acknowledgements

The authors would like to acknowledge the following colleagues at DLR Braunschweig, for their assistance in preparing and test flying the nonlinear autoflight controller: controller software implementer and ground simulator operator Dirk Leißling, safety pilot Hans-Jürgen Berns, experiment pilot Stefan Seydel, flight test engineer Michael Preß and flight engineer Regina Gebhard. Last but not least, we would like to acknowledge the “Programmdirektion Luftfahrt” of the German Aerospace Center DLR.

References

1. Realattas benchmark definition. Technical Report BRPR-CT98-0627/TP-04v1, REAL Consortium, 2000.
2. J.-M. Bauschat, D. Monnich, W. Willemsen, and G. Looye. Flight testing robust autoland control laws. In *AIAA Guidance, Navigation, and Control Conference and Exhibi*, number AIAA 2001-4208, 2001.
3. J.J Buchholz, J.-M. Bauschat, K.-U. Hahn, and H.J. Pausder. *AGARD CP -577 : Flight Simulation - Where are the Challenges?*, chapter ATTAS & ATTHeS in-flight simulators. Braunschweig, 1996.
4. D. Fischenberg. Attas in-air aerodynamikmodell. Institutsbericht IB 111-97/31, German Aerospace Center DLR, Institut fuer Flugmechanik, Braunschweig, September 1997.
5. M. Gerrits. Direct lift control for the cessna citation ii. Master's thesis, Eindhoven University of Technology, 1994.
6. W.W. Kelley. Simulator evaluation of a flight-path-angle control system for a transport airplane with direct lift control. Technical report NASA-TP-1116, NASA Langley Research Center, 1978.
7. M. Lauterbach and R. Luckner. Vergleich verschiedener regelstrategien für die stufenlose verstellung der hinterkantenklappen im landeanflug. In *Deutscher Luft- und Raumfahrtkongress*, pages 307 – 318, 2010. (in German).
8. T.J.J. Lombaerts. *Fault Tolerant Flight Control. A Physical Model Approach*. PhD thesis, Delft University of Technology, 2010.
9. T.J.J. Lombaerts, H.O. Huisman, Q.P Chu, J.A. Mulder, and D.A. Joosten. Nonlinear reconfiguring flight control based on on-line physical model identification. *AIAA Journal of Guidance, Control and Dynamics*, 32(3):727–748, May–June 2009 2009.
10. T.J.J. Lombaerts and G.H.N. Looye. Design and flight testing of manual nonlinear flight control laws. In *AIAA Guidance, Navigation and Control Conference and Exhibit*, number AIAA-2011-6469. American Insitutue of Aeronautics and Astronautics, 2011.
11. T.J.J. Lombaerts and G.H.N. Looye. Design and flight testing of nonlinear autoflight control laws. In *AIAA Guidance, Navigation and Control Conference and Exhibit*, number AIAA-2012-4982. American Insitutue of Aeronautics and Astronautics, 2012.
12. G. Looye and H.-D. Joos. Design of autoland controller functions with multiobjective optimization. *AIAA Journal of Guidance, Control and Dynamics*, 29(2):475–484, March-April 2006.
13. G.H.N. Looye. *An Integrated Approach to Aircraft Modelling and Flight Control Law Design*. PhD thesis, Delft University of Technology, 2007.
14. L.O. Lykken and N.M. Shah. Direct lift control for improved automatic landing and performance of transport aircraft. *Journal of Aircraft*, 9(5):325 – 332, May 1972.
15. Walter E. McNeill, Ronald M. Gerdes, Robert C. Innis, and Jack D. Ratcliff. A flight study of the use of direct-lift-control flaps to improve station keeping during in-flight refueling. Technical Memorandum TM X-2936, NASA Ames Research Center, Moffett Field, CA94035, October 1973.
16. J.A. Mulder and J.C. van der Vaart. *Aircraft responses to atmospheric turbulence*. Delft University of Technology, Faculty of Aerospace Engineering, Delft, The Netherlands, May 1998.
17. J.A. Mulder, W.H.J.J. van Staveren, J.C. van der Vaart, and E. de Weerdt. *AE3-302 Flight Dynamics, Lecture Notes*. Delft University of Technology, Faculty of Aerospace Engineering, Delft, The Netherlands, January 25 2006.
18. W.F.J.A. Rouwhorst. Robust and effcient autopilots control laws design, demonstrating the use of modern robust control design methodologies in the autoland system design process - the real project. In *Proceedings of the Aeronautics Days 2001*, Hamburg, Germany, January 2001.